Flow Boiling Heat Transfer and Two-Phase Flow Instability of Nanofluids in a Minichannel

Leyuan Yu
Department of Mechanical Engineering,
University of Houston,
Houston, TX 77204-4006

Aritra Sur
Department of Mechanical Engineering,
University of Houston,
Houston, TX 77204-4006

Dong Liu[1]
Department of Mechanical Engineering,
University of Houston,
Houston, TX 77204-4006
e-mail: dongliu@uh.edu

Single-phase convective heat transfer of nanofluids has been studied extensively, and different degrees of enhancement were observed over the base fluids, whereas there is still debate on the improvement in overall thermal performance when both heat transfer and hydrodynamic characteristics are considered. Meanwhile, very few studies have been devoted to investigating two-phase heat transfer of nanofluids, and it remains inconclusive whether the same pessimistic outlook should be expected. In this work, an experimental study of forced convective flow boiling and two-phase flow was conducted for Al_2O_3–water nanofluids through a minichannel. General flow boiling heat transfer characteristics were measured, and the effects of nanofluids on the onset of nucleate boiling (ONB) were studied. Two-phase flow instabilities were also explored with an emphasis on the transition boundaries of onset of flow instabilities (OFI). It was found that the presence of nanoparticles delays ONB and suppresses OFI, and the extent is correlated to the nanoparticle volume concentration. These effects were attributed to the changes in available nucleation sites and surface wettability as well as thinning of thermal boundary layers in nanofluid flow. Additionally, it was observed that the pressure-drop type flow instability prevails in two-phase flow of nanofluids, but with reduced amplitude in pressure, temperature, and mass flux oscillations. [DOI: 10.1115/1.4029647]

Keywords: nanofluids, flow boiling, onset of nucleate boiling, onset of flow instability, two-phase flow instability, heat transfer, minichannel

Introduction

Nanofluids are a new type of functional thermal fluid, which are usually formulated by dispersing nanoparticles with diameters smaller than 100 nm into a base fluid, such as water, mineral oil, and ethylene glycol. It was postulated that the addition of nanoparticles would drastically improve the thermal conductivity of the mixture, thereby making nanofluids a good candidate for high-performance applications for electronics cooling and thermal processing of materials [1–3]. Recent studies have revealed various degrees of enhancement in single-phase convective heat transfer of nanofluids over that of the base fluids [4–11]; however, there is still some debate on the improvement in the overall thermal performance when both heat transfer and hydrodynamic performances (e.g., pressure drop and pumping power) are considered collectively [12–18]. Naturally, the subsequent question arises: How will the phase-change heat transfer be affected in nanofluids?

In contrast to the vast body of literature on thermophysical properties and single-phase heat transfer of nanofluids, there are only scant studies on pool boiling heat transfer and even fewer on flow boiling and two-phase flow of nanofluids [19–39]. Das et al. [19–21] investigated the pool boiling characteristics of Al_2O_3–water nanofluids on cylindrical heaters, and they observed the boiling heat transfer is inferior to that of the base fluid. Similar findings of heat transfer deterioration were documented by Bang and Heung Chang [26] and Kim et al. [35] in their respective studies of pool boiling of Al_2O_3–water nanofluids. On the other hand, Narayan et al. [22] found the pool boiling heat transfer of Al_2O_3–water nanofluids is significantly enhanced on a rough heater surface (surface roughness $R_a = 524$ nm) but is retarded on a smooth surface ($R_a = 48$ nm). Wen and Ding [25] reported dramatic increase in nucleate boiling heat transfer with Al_2O_3–water nanofluids and showed the heat transfer enhancement is proportional to the nanoparticle concentration and the applied heat flux. Liu et al. [29] measured pool boiling heat transfer of CuO–water nanofluids, and they identified an optimum nanoparticle concentration that yields the maximum heat transfer enhancement, beyond which boiling heat transfer is reduced. In the study of flow boiling of carbon nanotube (CNT)–water nanofluids, Park and Jung [31] observed that the boiling heat transfer is augmented at low heat fluxes and the enhancement deteriorates as the heat flux increases, whereas Xue et al. [32] discovered that the addition of CNTs only suppresses the flow boiling heat transfer.

The brief literature survey above reveals a clear discrepancy regarding the effects of nanofluids on boiling heat transfer. More interestingly, both the heat transfer enhancement and deterioration were attributed to the sedimentation/deposition of nanoparticles on the boiling surface, which modifies the surface wettability and the distribution of active nucleation sites. Nevertheless, the detailed physical mechanisms remain missing. Hence, there is a need for more thorough experimental investigations to clarify the existing disparities and to, eventually, advance the understanding of boiling heat transfer and two-phase flow of nanofluids. In this work, an experimental study of forced convective flow boiling and two-phase flow was conducted for Al_2O_3–water nanofluids through a minichannel with the following specific goals: (1) to explore the flow boiling heat transfer characteristics; (2) to study the effects of nanofluids on the ONB; and (3) to investigate two-phase flow instabilities and study the effects of nanofluids on the transition boundaries of the OFI.

Preparation of Nanofluids

Al_2O_3–water nanofluids with two nanoparticle volume concentrations (0.01 vol. % and 0.1 vol. %) were used in this work. They were prepared following the same method described in Ref. [40],

[1]Corresponding author.

Contributed by the Heat Transfer Division of ASME for publication in the Journal of Heat Transfer. Manuscript received June 16, 2014; final manuscript received January 10, 2015; published online February 10, 2015. Assoc. Editor: Robert D. Tzou.

except that the de-ionized (DI) water was degassed by vigorously boiling for 2 hr before being mixing with Al_2O_3 nanoparticles. After degassing, the amount of dissolved air in water was monitored with an oxygen sensor (Oakton DO 600). If the degassed water was left unattended in the container, the air concentration increased gradually from 3.6 mg/L to a stable value of 7.7 mg/L at the end of a 24-hr period. The actual amount of air dissolved in the nanofluids was not directly measured to avoid the contamination of the oxygen sensor, but it was expected to be much lower than 7.7 mg/L since a sonication process was used in the nanofluid synthesis. According to Ref. [41], when the concentration of dissolved oxygen is lower than 5.4 mg/L, the effect of dissolved air on boiling heat transfer can be safely neglected. This is expected to be the case for the present study.

Experiments

The experimental loop for the flow boiling heat transfer study of nanofluids is shown in Fig. 1. A gear pump (IDEX Micropump 67-GA-V21) was used to circulate the nanofluids through the test loop. The volumetric flow rate was measured by a turbine flowmeter (McMillan G111). A liquid–liquid heat exchanger (Lytron LL520G14) was used together with an air-cooled chiller (Neslab MERLIN 25) to reduce the temperature of the heated nanofluid to room temperature before it flows back to the reservoir. A proportional integral derivative-regulated preheater (Infinity CRES-ILB-24-0040-K) was instrumented to control the inlet subcooling. A control valve was installed near the exit of the test section to reduce possible feedbacks from the compressible volumes in the downstream piping system (such as the heat exchanger and the reservoir). Additionally, a drainage tank was installed after the throttle valve to help remove dissolved gas, if any, escaping from the working fluid during the preheating stage before the flow boiling experiment starts.

The test tube is a circular minichannel made of stainless steel (type 304). It measures 1.09 mm in inner diameter (D), 0.25 mm in wall thickness, and 306 mm in total length. The minichannel is resistively heated by passing a DC current through it. The voltage drop across the channel was measured by the data acquisition system (Agilent 34970A), and the current was obtained by using a shunt resistor. Six copper-constantan (T-type) thermocouples (Omega 5TC-TT-T40-36) were attached to the outer wall of the channel at 44 mm axial intervals (TC1 through TC6). Temperature readings from these thermocouples, $T_{w,o}$, were extrapolated to yield the local temperatures, T_w, at the inner wall of the channel [40]

$$T_w = T_{w,o} + \frac{\rho_f Q C_p (T_{f,out} - T_{f,in})}{4\pi k_w L} - \frac{\rho_f Q C_p (T_{f,out} - T_{f,in}) D_o^2}{2\pi k_w (D_o^2 - D^2) L} \ln \frac{D_o}{D} \quad (1)$$

where D_o is the outer diameter of the tube ($D_o = 1.59$ mm). To minimize heat loss to the ambient, the test tube was wrapped with multiple layers of thermal insulating materials. Two thermocouple probes (Omega TMT IN-020G-6) were used to measure the fluid temperatures at the inlet and outlet of the channel. Two absolute pressure transducers (Omega PX319-050A5V and PX319-030A5V) were used to measure the pressure drop across the channel. The integrity of the experimental apparatus has been validated by the single-phase heat transfer experiments reported in Refs. [14,40,42].

The test procedures for the flow boiling heat transfer experiments are as follows. The gear pump was first started to circulate the working fluid at the desired flow rate. The preheater was then activated, and it usually took about 60 min for the fluid to reach the target temperature at the inlet of the minichannel. Afterward, the DC power supply was turned on at the lowest power input level. A steady state was reached when the readings from all thermocouples remained stable (within $\pm 0.3\,^{\circ}C$) for at least 5 min. The measured parameters, including the flow rate, pressure, temperate, and applied voltage, and current, were read into a data acquisition system (Agilent 34970A), and each measurement value was calculated as an average of 300 readings. Following that, the power input was increased with a small increment, and the procedure repeated for subsequent experiments. In the experiments reported here, the inlet temperature of the test fluid ranged from 80.4 to 90.6 °C, the maximum heat flux achieved was 40.6 W/cm^2, and the maximum thermodynamic quality at the exit was 0.05. (Note: despite this low thermodynamic quality, the corresponding vapor void fraction is not necessarily so low, especially under subcooled flow conditions. Thus, the flow in the minichannel may still encompass the major two-phase regimes, which, unfortunately, cannot be visualized with the present experimental apparatus. However, the experimental results will show that, even at this quality range, the two-phase flow instability is strongly affected by the nanofluids.)

Similar procedures were followed for the two-phase flow instability experiments except that the power input level was first fixed, and the flow rate was gradually reduced from the maximum value for subsequent tests. After reaching the minimum flow rate, one set of two-phase flow instability studies was done and the power input was then adjusted to a new level to repeat the above process.

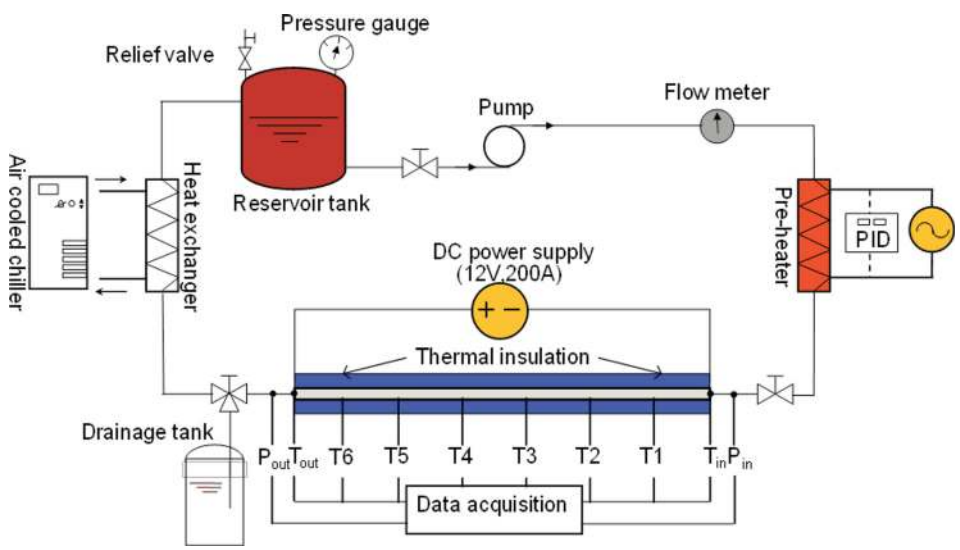

Fig. 1 Schematic of the experimental apparatus

The corresponding mass flux tested in the experiments ranged from 680 to 3100 kg/m^{2}s.

To evaluate the effect of the wettability of the working fluid, the contact angle (θ) was measured for the nanofluids on a flat stainless steel plate (type 304) using the sessile-drop method with a tensiometer (KSV CAM101). Prior to each measurement, the test plate was cleaned with acetone, rinsed thoroughly with DI water, and then air-dried with nitrogen. A 2-μl droplet of sample fluid was first deposited gently with a syringe vertically down onto the test plate. When the droplet reached the equilibrium state, its image was captured by a CCD camera. The outer profile of the droplet was then curve-fitted using builtin image processing software, and the contact angle was calculated from the Young–Laplace theory [43]. The results suggest that the contact angle of nanofluids is smaller than that of water and decreases with the nanoparticle volume concentration. The measured contact angles were 85.9 deg, 82.7 deg, and 76.0 deg for water, 0.01 vol. % and 0.1 vol. % Al_2O_3–water nanofluid, respectively. The measurements are in agreement with the previous results in the literature [35,44–47].

In this work, three different test samples were experimented upon: DI water, 0.01 vol. % and 0.1 vol. % Al_2O_3–water nanofluids. To avoid the difficulties in quantifying the effects of particle deposition on flow boiling and two-phase flow, the minichannel test tube was replaced with a new one after each test with a sample nanofluid, and the subsequent experiment was conducted in the fresh channel. The main reasons for doing so include: (1) It is difficult to determine whether/when an *equilibrium* state will be reached for the continuous nanoparticle deposition process; (2) It is not straightforward to evaluate the morphological properties (such as the thickness and surface roughness) of the coating layer deposited inside a minichannel; and (3) it is even more challenging to ensure the surface parameters are consistent at different nanoparticle concentrations and inlet flow velocities. Therefore, the experiments were performed in fresh channels, assuming that the particle buildup process is relatively slow at the low nanoparticle concentrations considered in this work and the effect is limited to changing the nucleation site distribution and varying the surface wettability.

Data Reduction

Heat loss from the test section to the ambient was first estimated under single-phase heat transfer condition, i.e., from the difference between the total power input and the sensible heat gain by the fluid

$$q_{\text{loss}} = q_{\text{input}} - \dot{m}c_{\text{p}}\left(T_{\text{f,out}} - T_{\text{f,in}}\right) \tag{2}$$

Since the heat loss is caused primarily by natural convection, which is driven by the temperature difference between the channel wall and the ambient, q_{loss} was correlated conveniently as a function of the average wall temperature ($\bar{T}_{\text{w}} = \sum_{i=1}^{6} T_i/6$): $q_{\text{loss}} = q_{\text{loss}}(\bar{T}_{\text{w}})$ [40]. This correlation was then extrapolated to obtain heat loss under the flow boiling conditions. The applied heat flux q''_{w} was calculated based on the inner area of the minichannel ($A = \pi \cdot D \cdot L$)

$$q''_{\text{w}} = \left(q_{\text{input}} - q_{\text{loss}}\right)/A \tag{3}$$

Temperature-dependent properties were used for water and nanofluids in the data analysis [40,42], and are not repeated herein for brevity.

The measurement uncertainties for the temperature, the flow rate, and the pressure drop were $\pm 0.3\,^{\circ}$C, 1% of full scale and 2% of full scale, respectively. A standard error analysis [48] revealed that the uncertainties in the reported heat flux and mass flux were in the ranges of 5.2–13.8% and 1.6–3.5%, respectively. The data reduction methods have been validated by single-phase heat transfer experiments as in Refs. [14,40,42].

Results and Discussion

Boiling Curves. Boiling curves were constructed for water and nanofluids using the wall temperatures measured at the six streamwise locations. Figure 2 shows that at low heat fluxes, single-phase heat transfer prevails in the test fluids, and the steeper slope of the curves obtained from the upstream thermocouples (T_1, T_2, and T_3) clearly indicate the entrance region effect (i.e., higher convective heat transfer coefficient). When the heat flux is increased, the slope first changes in the measurement from T_6, indicating that the ONB occurs near the exit of the test tube and then gradually propagates upstream. Another important discovery is that ONB in the nanofluids takes place at higher heat fluxes and greater wall superheat values in proportion to the nanoparticle concentration. For instance, the ONB at the T_6 location occurs at $q''_{\text{w}} = 10.4$ W/cm^2 and $T_{\text{w}} = 104.1\,^{\circ}$C for water, whereas it is delayed to $q''_{\text{w}} = 10.8$ W/cm^2 and $T_{\text{w}} = 105.3\,^{\circ}$C for 0.01 vol. % nanofluid, and $q''_{\text{w}} = 18.4$ W/cm^2 and $T_{\text{w}} = 125.3\,^{\circ}$C for 0.1 vol. % nanofluid, respectively.

ONB. The boiling curves in Fig. 2 show that ONB occurs at higher heat fluxes as the nanoparticle concentration increases. The delayed ONB can be distinguished more clearly from Fig. 3 where the *global* boiling curves are constructed using the average wall temperature $\bar{T}_{\text{w}}$. It is worth noting that the use of average wall temperature does not imply the entire test section is in a specific two-phase flow regime with little change in wall temperature along the channel length, but rather, it is intended to highlight the transition point from single- to two-phase heat transfer, as described below. Figure 3 shows that the experimental data for all test fluids collapse together onto one single curve in the single-phase flow region, due to the insignificant effect of dilute particle concentrations on the thermophysical properties of nanofluids. However, the data start to deviate from the single-phase trendline in an order corresponding to the nanoparticle concentrations: first, water, then 0.01 vol. % nanofluid and, last, 0.1 vol. % nanofluid. Therefore, the difference in ONB and the ensuing two-phase heat transfer between water and the nanofluids must be induced by factors other than the apparent thermophysical properties.

Similar findings of delayed ONB were reported in pool boiling heat transfer experiments of nanofluids [49,50]. However, no previous studies have investigated the characteristics of ONB of nanofluids in forced convective flow boiling. Furthermore, as will be discussed later, the retarded boiling incipience plays an important role in the flow boiling instabilities. Therefore, the possible mechanisms for the delayed ONB are discussed in the following text.

It is hypothesized that two primary mechanisms are responsible for the delayed ONB in flow boiling of nanofluids in this work:

(1) The nanoparticle layer deposited on the wall surface may alter the profile of active nucleation sites. It was reported that once boiling takes place, nanoparticles first aggregate at the liquid–vapor interface, and then quickly adhere to the wall surface [30]. As depicted in Fig. 4, smaller-sized cavities will be completely filled by the nanoparticle aggregates while the larger ones may be partially filled. Consequently, the size range and number density of *available* nucleation sites will diminish, making the ONB more difficult to occur. (Note that: Ref. [22] postulates if the size of nanoparticles is smaller than or comparable to the surface roughness, they may increase the number of active nucleation sites by splitting a single site into multiple ones. In the present work, the roughness-to-particle-size ratio was not quantified, but the ONB results do not seem to support this postulation.)

(2) From previous single-phase heat transfer studies [8,11,40,42,51–53], it is known that the development of thermal boundary layer is retarded in nanofluids, i.e., the

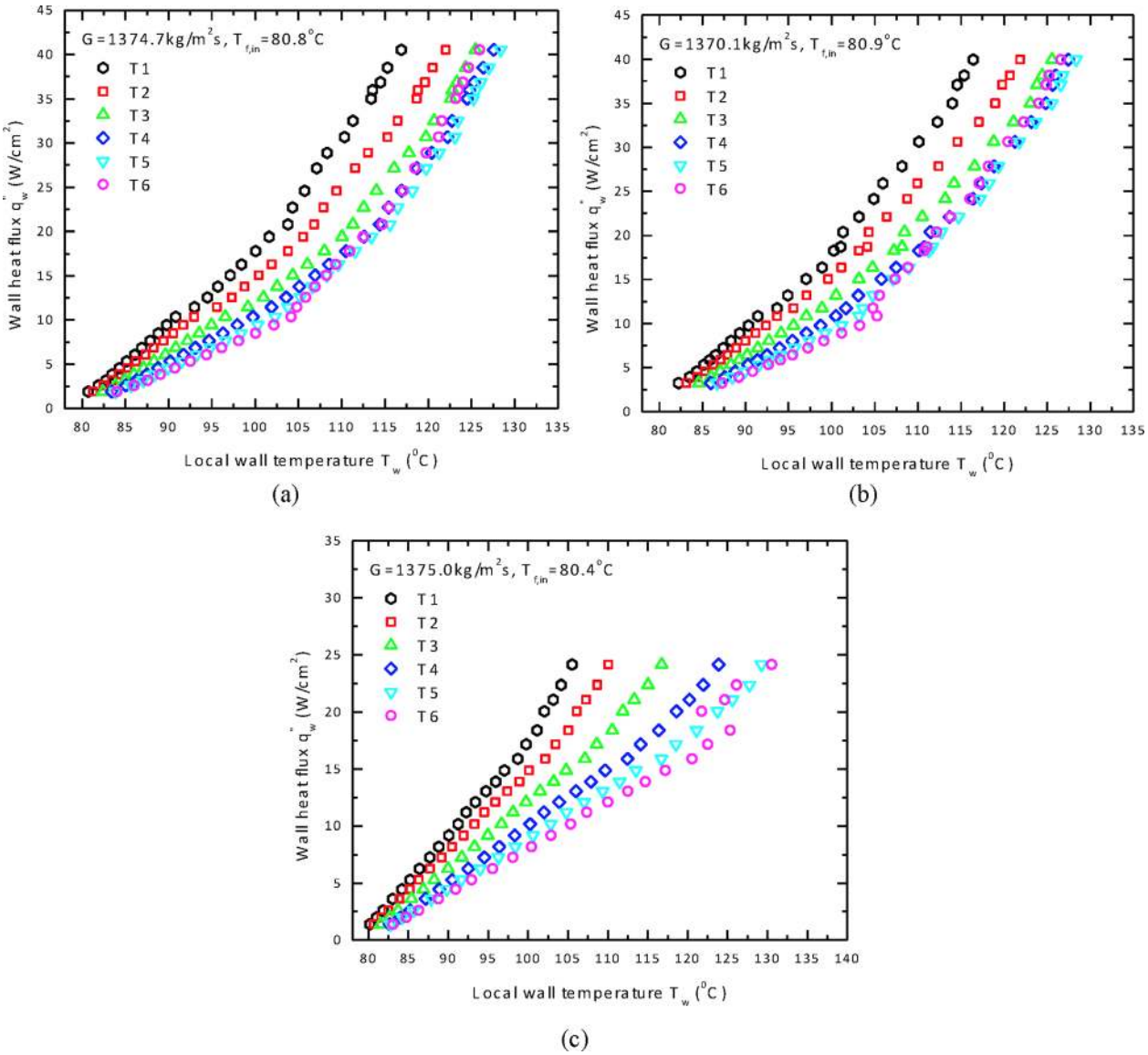

Fig. 2 Boiling curves of (*a*) water, (*b*) 0.01 vol. % nanofluid, and (*c*) 0.1 vol. % nanofluid

thermal boundary layer becomes thinner in nanofluids, due to the effect of the shear-induced nanoparticle migration on the effective viscosity and thermal conductivity. In the classical ONB model [54], Hsu showed that the size range of theoretically *eligible* nucleate cavities depends proportionally on the thickness of the thermal boundary layer. Therefore, suppressed thermal boundary layer will result in less active nucleation sites in flow boiling of nanofluids.

In addition, ONB is strongly dependent on the wettability of the boiling surface, which can be represented by the contact angle that the fluid makes at the liquid–solid contact [55]. Using the ONB models in the literature [54,56–60], the size range of active nucleation sites is shown to be a function of θ,

$$r_{c,min} \le r_c \le r_{c,max} \tag{4}$$

where

$$r_{c,min,max} = r^* \pm \sqrt{\left(T_w + \frac{2\sigma C}{\rho_v h_{fg}}\frac{q''_w}{k_f} - T_s\right)^2 - 4\frac{2\sigma C}{\rho_v h_{fg}}\frac{q''_w}{k_f}T_w} \times \frac{\sin\theta}{1+\cos\theta}\Big/\left(2\frac{q''_w}{k_f}\right) \tag{5}$$

and

$$r^* = \left(T_w + \frac{2\sigma C}{\rho_v h_{fg}}\frac{q''_w}{k_f} - T_s\right)\frac{\sin\theta}{1+\cos\theta}\Big/\left(2\frac{q''_w}{k_f}\right) \tag{6}$$

$$C = 1 + \cos\theta \tag{7}$$

Only cavities with a radius r_c falling in the size range defined by Eq. (4) can be active. From the contact angle measurements, the contact angles were 85.9 deg, 82.7 deg, and 76.0 deg for water, 0.01 vol. % and 0.1 vol. % Al_2O_3–water nanofluid, respectively. Figure 5 shows the size range of active nucleation sites corresponding to these contact angle values and a hypothetical case ($\theta = 20$ deg) as a function of the wall temperature. Clearly, the size range diminishes as the contact angle decreases (i.e., as the nanoparticle concentration increases from 0 to 0.1 vol. %), and the critical wall temperature required to initiate ONB increases quickly when there are lesser active nucleation sites available. The results in Fig. 5 provide another proof that the ONB is delayed in this work when Al_2O_3–water nanofluids are used as the working fluid.

Two-Phase Flow Instability. In this work, experiments were conducted to investigate the effect of nanofluids on the two-phase

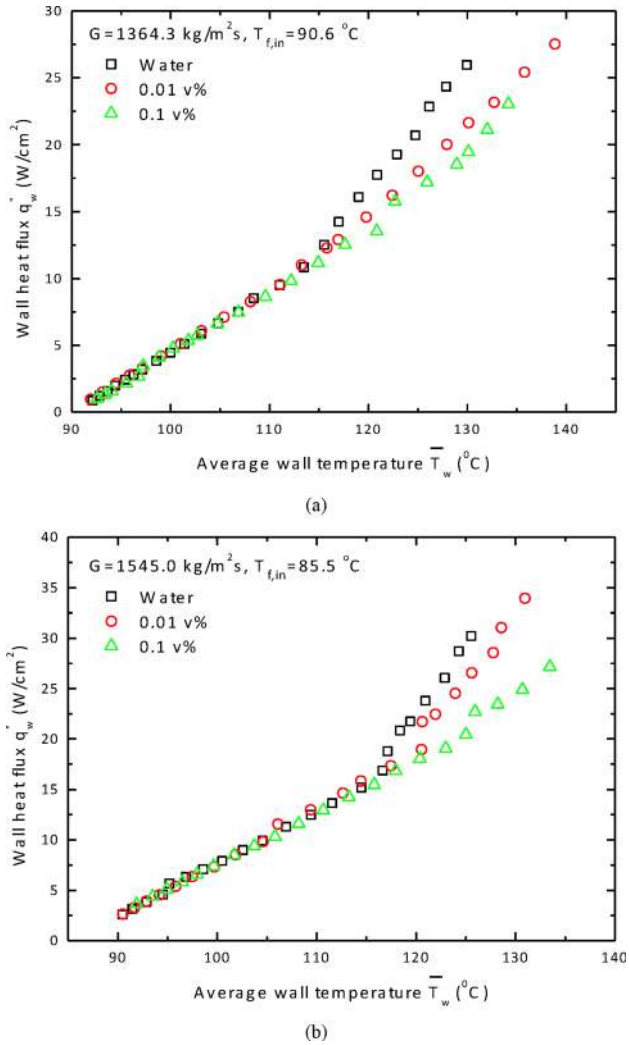

Fig. 3 Comparison of the boiling curves at two inlet conditions: (*a*) $G = 1364.3\,\text{kg/m}^2\text{s}$, $T_{f,in} = 90.6\,^\circ\text{C}$ and (*b*) $G = 1545.0\,\text{kg/m}^2\text{s}$, $T_{f,in} = 85.5\,^\circ\text{C}$

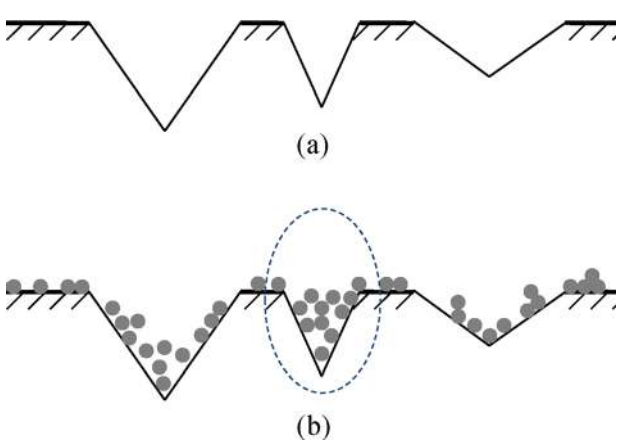

Fig. 4 Distribution of nucleation sites on a boiling surface (*a*) before and (*b*) after the deposition of nanoparticles

flow instabilities in flowing boiling through the minichannel test section.

Small-scale fluctuations in a two-phase flow system, such as two-phase interfacial waves and oscillations in flow rate and system pressure, may trigger large-scale flow instabilities. The

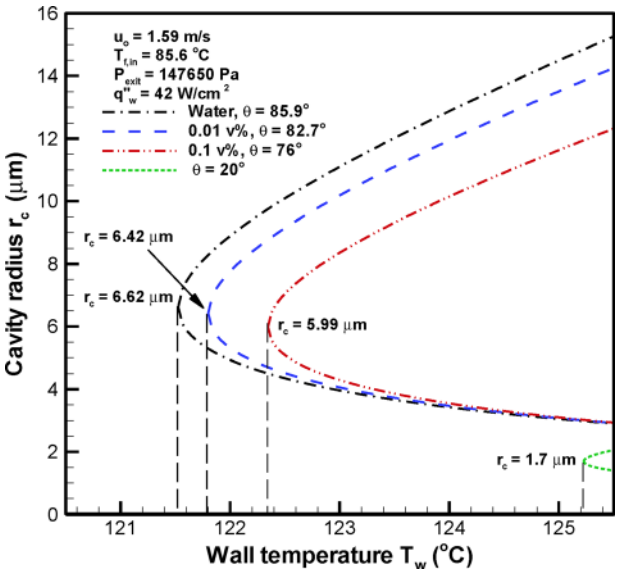

Fig. 5 Size range of active nucleation sites as a function of wall temperature for different contact angles (Note: $\theta = 20$ deg is a hypothetical case to illustrate the effect of contact angle)

two-phase flow instabilities are undesirable because severe flow rate/pressure/temperature oscillations can change a steady heat transfer process to go beyond the designed safety regime of the heat transfer equipments. Additionally, the periodic cycling of the wall temperature will induce thermal stress in the wall material that may build up and eventually lead to mechanical breakdown [61]. Therefore, it is important to suppress the two-phase flow instabilities in flow boiling systems, especially for microchannel/minichannel heat exchangers as the two-phase instability has largely prevented their wide-spread application in industry [62].

Two-phase flow instability usually arises from the interactions between the internal and external flow characteristics, and can be classified into two categories: static instability and dynamic instability [55,63,64]. Static instability occurs when the new operating conditions of the disturbed two-phase flow system tend asymptotically toward the ones that are different from the original ones (e.g., Ledinegg instability is the most common static instability). Dynamic instability is more relevant to the present study, which takes place when the interaction and delayed feedback between the inertia of flow and compressibility of the two-phase mixture play a major role in stimulating the instability. There are three primary types of dynamic instabilities [64,65], namely, density-wave type oscillation, pressure-drop type oscillation, and thermal oscillation (Note: since acoustic oscillation often has little effect on two-phase flow [55], it is not considered in this work.)

(1) Density-wave oscillations are caused by multiple regenerative feedbacks between the mass flux, vapor generation rate, and two-phase pressure drop [64,66], during which fluid waves of mixtures of alternately higher and lower density (i.e., liquid and vapor) travel along the flow channel. The oscillation amplitudes and periods of mass flux, pressure, and wall temperature are usually small, and the oscillations of mass flow rate and pressure are in phase [67].
(2) Pressure-drop type oscillations occur when a significant amount of compressible volume exists in the two-phase flow system [61]. The compressible volume serves as the buffer zone where there is an imbalance in the internal and external mass flux versus pressure-drop characteristics. The compressible volume can be produced if the flow channel has a long aspect ratio (e.g., $L/D > 150$) under low mass flux and/or high heat flux conditions [68] a surging tank/ accumulator is installed upstream of the boiling channel [67,69–71]. Pressure-drop type oscillations are

characterized by long-period, large-amplitude oscillations of pressure, mass flux, and wall temperatures. Generally, the fluctuations of mass flux and pressure are out of phase [67,72].

(3) Thermal oscillations are related to the instability of the liquid film next to the channel wall. The flow usually oscillates between annular flow, transition boiling, and droplet flow. Large-amplitude fluctuations are often found in the wall temperature, while the periods and amplitudes of pressure and mass flux fluctuations are very small. Density-wave oscillations are required to trigger the thermal oscillations.

The three major dynamic instabilities are generally distinct from each other without overlap. Pressure-drop type oscillations usually start first. As the mass flux is reduced, the pressure in the channel increases to compress the vapor phase. Density-wave oscillations then occur when the compressible volume diminishes. Finally, thermal oscillations will ensue.

As a baseline case, Fig. 6 shows the time-dependent variation of six parameters of water flow, including the mass flux (G), inlet and out pressures (P_{in} and P_{out}), pumping power (P), and inlet and outlet temperatures (T_{in} and T_{out}), at two different test conditions. In Fig. 6(*a*), the mass flux is relatively high ($G = 2038.7\,kg/m^2s$), and the two-phase system operates in the stable flow region. The fluctuations in the data have no detectable amplitude and period, and are merely due to random noise. When G decreases to $1054.4\,kg/m^2s$, two-phase flow oscillations occur where all flow parameters demonstrate clear periodic peak-valley cycles, as depicted in Fig. 6(*b*). It is noticed that the oscillations of the mass flux and the inlet pressure are out of phase with a phase angle of 180 deg, and the oscillation period (about 6–7 s) is rather long as compared to the time needed for the fluid to pass through the channel (about 0.28 s), which are all typical features of the pressure-drop type instabilities. This is not surprising because the intrinsic conditions to trigger pressure-drop type oscillations do exist in the present two-phase flow system. First, the minichannel has a large aspect ratio of $L/D = 281$, which exceeds the threshold value for a "long tube" ($L/D \sim 150$), so the vapor phase generated in boiling provides sufficient amount of compressible volume. Second, the preheater located upstream to the test channel serves as a surge tank that can modulate the internal and external pressure drop versus mass flux characteristics.

The measurements of two-phase flow instabilities for 0.01 vol. % and 0.1 vol. % nanofluids are shown in Figs. 7 and 8. As compared to the results of water in Fig. 6, the oscillation amplitudes are smaller in both cases, and the periods are less distinguishable even at the lower mass fluxes where the pressure-drop type oscillations dominate in two-phase flow of water. The results suggest that two-phase flow oscillations are suppressed in nanofluids, and the extent of suppression increases as the particle concentration increases from 0.01 vol. % to 0.1 vol. %.

The suppression of two-phase flow instabilities in nanofluids can be better illustrated in Fig. 9. This plot is constructed using the instantaneous measurements of pressure drop (dP) and mass flux (G) over a period of 85 s as the coordinates. The set (nominal) mass flux was $1065.9\,kg/m^2s$ for all three fluids. An elliptical limit loop can be clearly identified from the water data, which indicates a well-defined oscillatory pattern of the pressure-drop type instability, where the magnitude of the pressure drop oscillates between 74.8 kPa and 102.4 kPa ($\Delta(dP) \sim 27$ kPa) and the mass flux between $1005.8\,kg/m^2s$ and $1105.9\,kg/m^2s$ ($\Delta G \sim 100\,kg/m^2s$). In contrast, the data points for nanofluids of both concentrations are clustered together with much less scatter ($\Delta(dP) \sim 10$ kPa and $\Delta G \sim 20\,kg/m^2s$). The suppressed fluctuations in pressure drop and mass flux are consistent with the observations in Figs. 7 and 8.

Two-phase flow instabilities of nanofluids were also studied under different heat fluxes. In the experiments, for each given heat flux, the flow rate was gradually reduced from the maximum value till the minimum value was reached. The internal characteristics

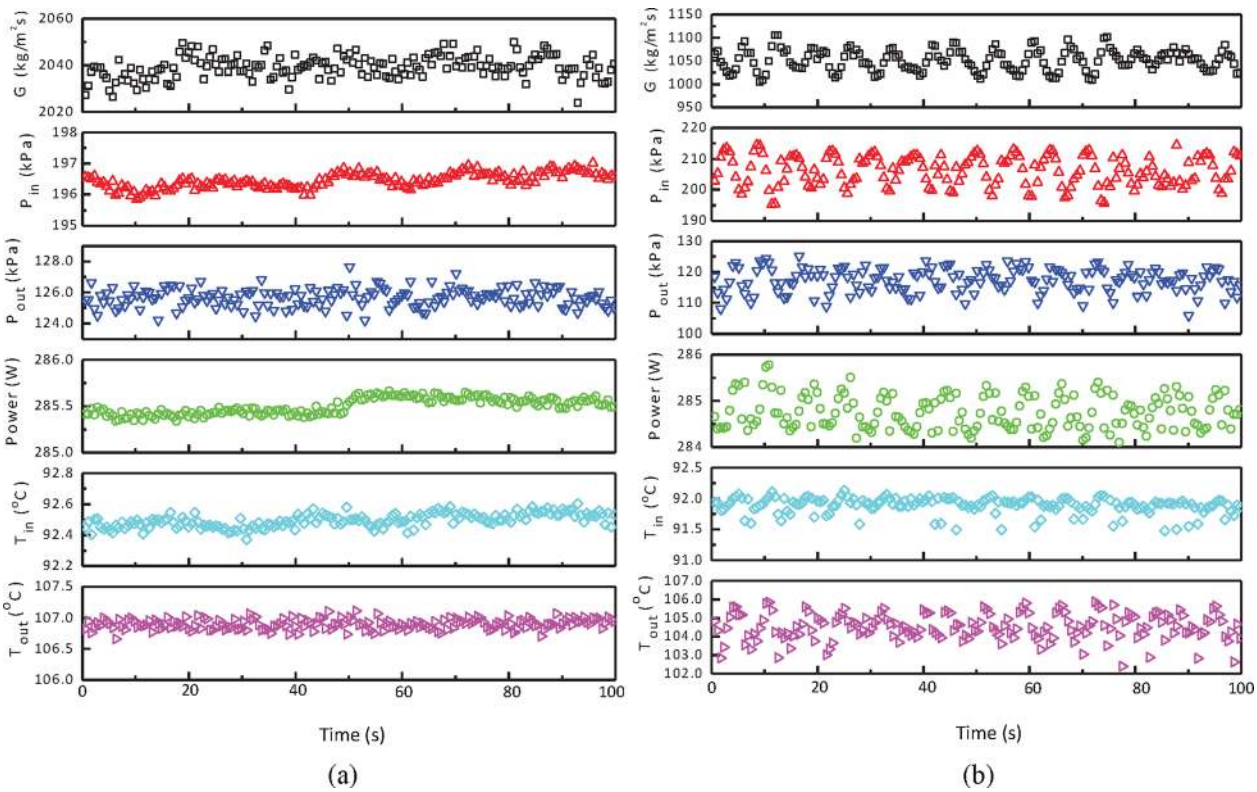

Fig. 6 Time-dependence of mass flux (G), inlet and outlet pressures (P_{in} and P_{out}), pumping power (P), and inlet and outlet temperatures (T_{in} and T_{out}) of water at (*a*) $G = 2038.7\,kg/m^2s$, $T_{f,in} = 92.3\,°C$, and $q''_w = 29.9\,W/cm^2$ (stable region); and (*b*) $G = 1054.4\,kg/m^2s$, $T_{f,in} = 91.9\,°C$, and $q''_w = 29.9\,W/cm^2$

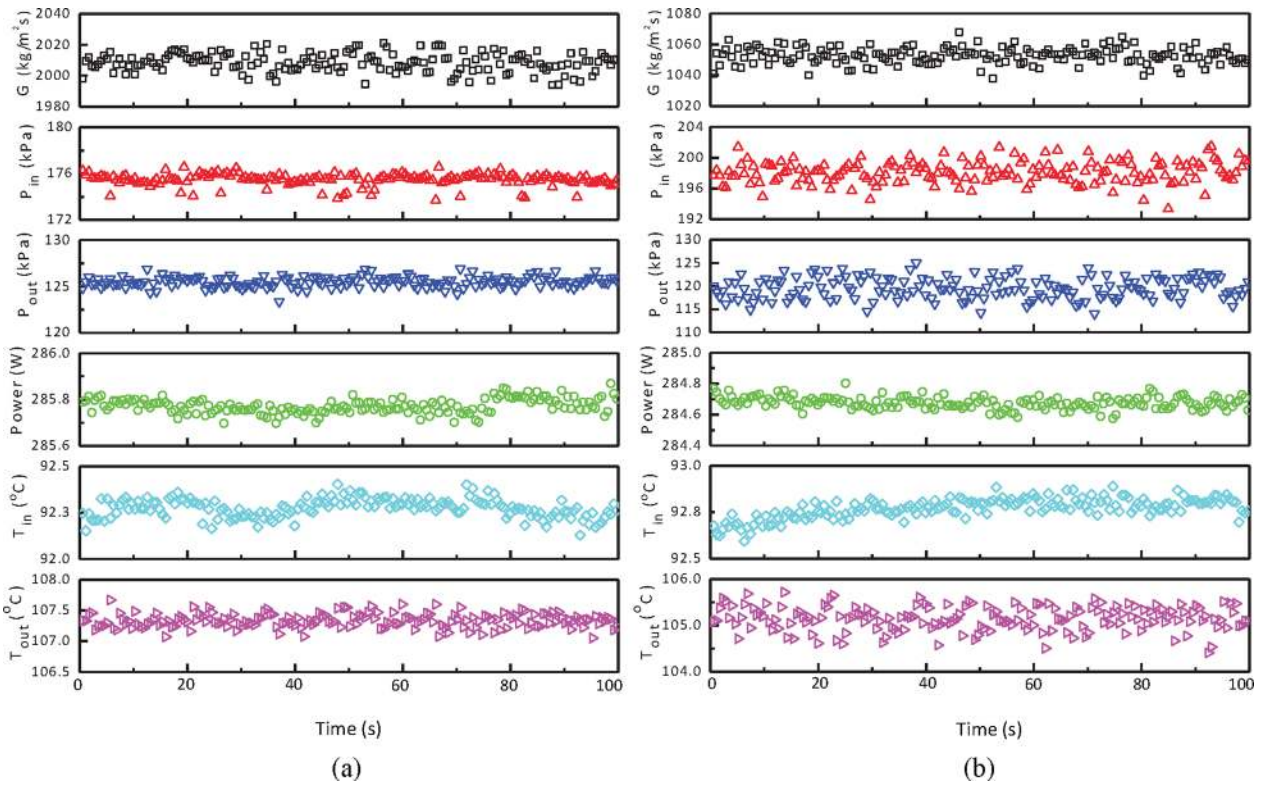

Fig. 7 Time-dependence of mass flux (G), inlet and outlet pressures (P_{in} and P_{out}), pumping power (P), and inlet and outlet temperatures (T_{in} and T_{out}) of 0.01 vol. % nanofluids at (*a*) $G = 2007.4\ kg/m^2s$, $T_{f,in} = 92.3\ ^\circ C$, and $q''_w = 29.9\ W/cm^2$ (stable region); and (*b*) $G = 1052.4\ kg/m^2s$, $T_{f,in} = 92.7\ ^\circ C$, and $q''_w = 29.9\ W/cm^2$

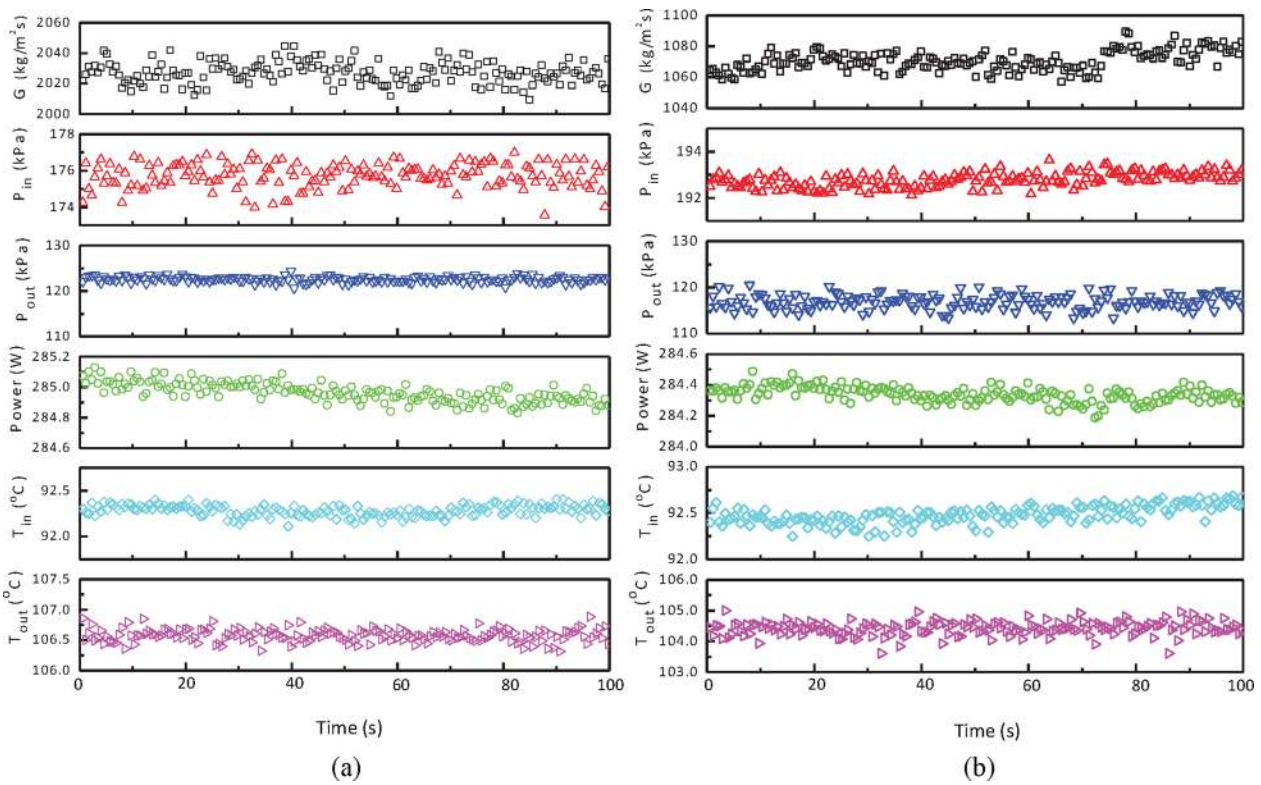

Fig. 8 Time-dependence of mass flux (G), inlet and outlet pressures (P_{in} and P_{out}), pumping power (P), and inlet and outlet temperatures (T_{in} and T_{out}) of 0.1 vol. % nanofluids at (*a*) $G = 2028.5\ kg/m^2s$, $T_{f,in} = 92.3\ ^\circ C$, and $q''_w = 29.9\ W/cm^2$ (stable region); and (*b*) $G = 1065.9\ kg/m^2s$, $T_{f,in} = 92.5\ ^\circ C$, and $q''_w = 29.9\ W/cm^2$

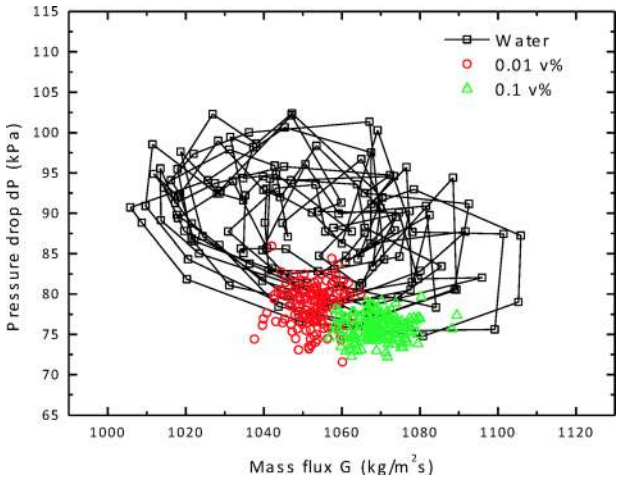

Fig. 9 Two-phase flow oscillations at $G = 1065.9\,\text{kg/m}^2\text{s}$, $T_{f,in} = 91.9\text{–}92.5\,^\circ\text{C}$, and $q''_w = 29.9\,\text{W/cm}^2$

of the two-phase flow are presented in terms of the pressure drop versus mass flux plot as shown in Fig. 10. Taking water, for example (Fig. 10(*a*)), the flow starts off as single-phase liquid at the highest mass flux, and the pressure drop gradually decreases as the mass flux reduces. Depending on the applied heat flux, the data will deviate from the single-phase line (represented by the curve corresponding to $q''_w = 0\,\text{W/cm}^2$) at a certain mass flux, which denotes the ONB and the commencement of two-phase flow. The decreasing trend of the pressure-drop curve persists and the two-phase flow remains stable till a point where further decreasing the mass flux causes the pressure drop to rebound quickly, due to intensified vaporization in the test channel. Afterward, the slope of the data line changes from positive to negative, and two-phase flow oscillations will be observed. This threshold point demarcates the transition from stable to unstable two-phase flow, and is defined as the OFI. At elevated heat fluxes, the OFI shifts to higher threshold mass fluxes. Connecting all the threshold points yields the OFI boundary (shown as the dashed lines on Fig. 10(*a*)), i.e., the region to its left is unstable and the region to its right is stable.

Similar plots are presented in Figs. 10(*b*) and 10(*c*) for nanofluids. As the nanoparticle concentration increases, the OFI boundary line draws closer to the single-phase line, indicating a diminishing stable region. Further examination of the results reveals two interesting features. First, the OFI threshold values of mass flux for nanofluids decrease considerably as compared to that of water. Second, the data points of nanofluid flow stay on the single-phase line ($q''_w = 0\,\text{W/cm}^2$) over a wider range of mass fluxes, and then transition into the unstable two-phase region occurs almost immediately (Fig. 11(*c*)). Therefore, it can be

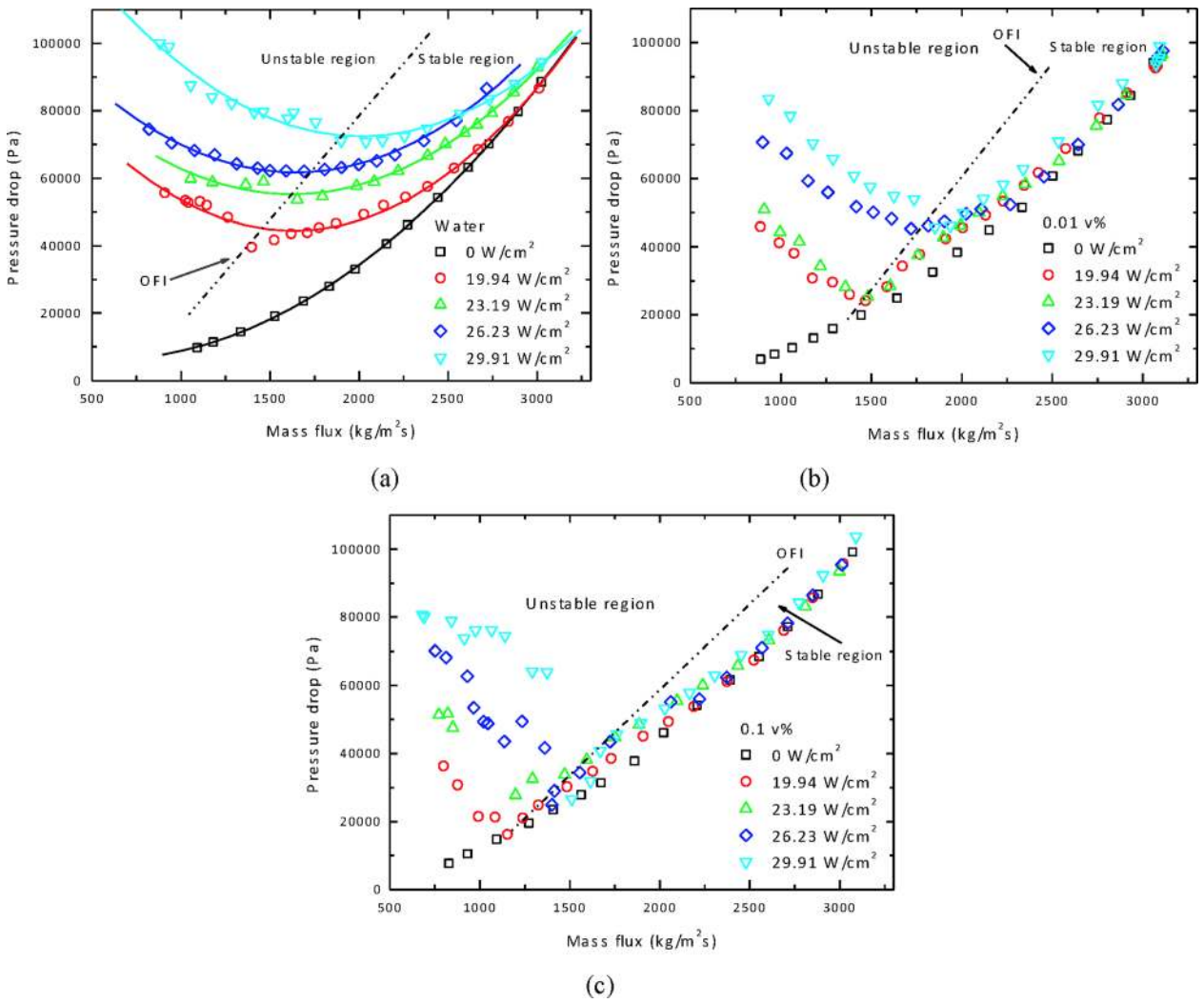

Fig. 10 Two-phase flow characteristics under different heat fluxes: (*a*) water, (*b*) 0.01 vol. % nanofluid, and (*c*) 0.1 vol. % nanofluid ($T_{f,in} = 92.5\,^\circ\text{C}$)

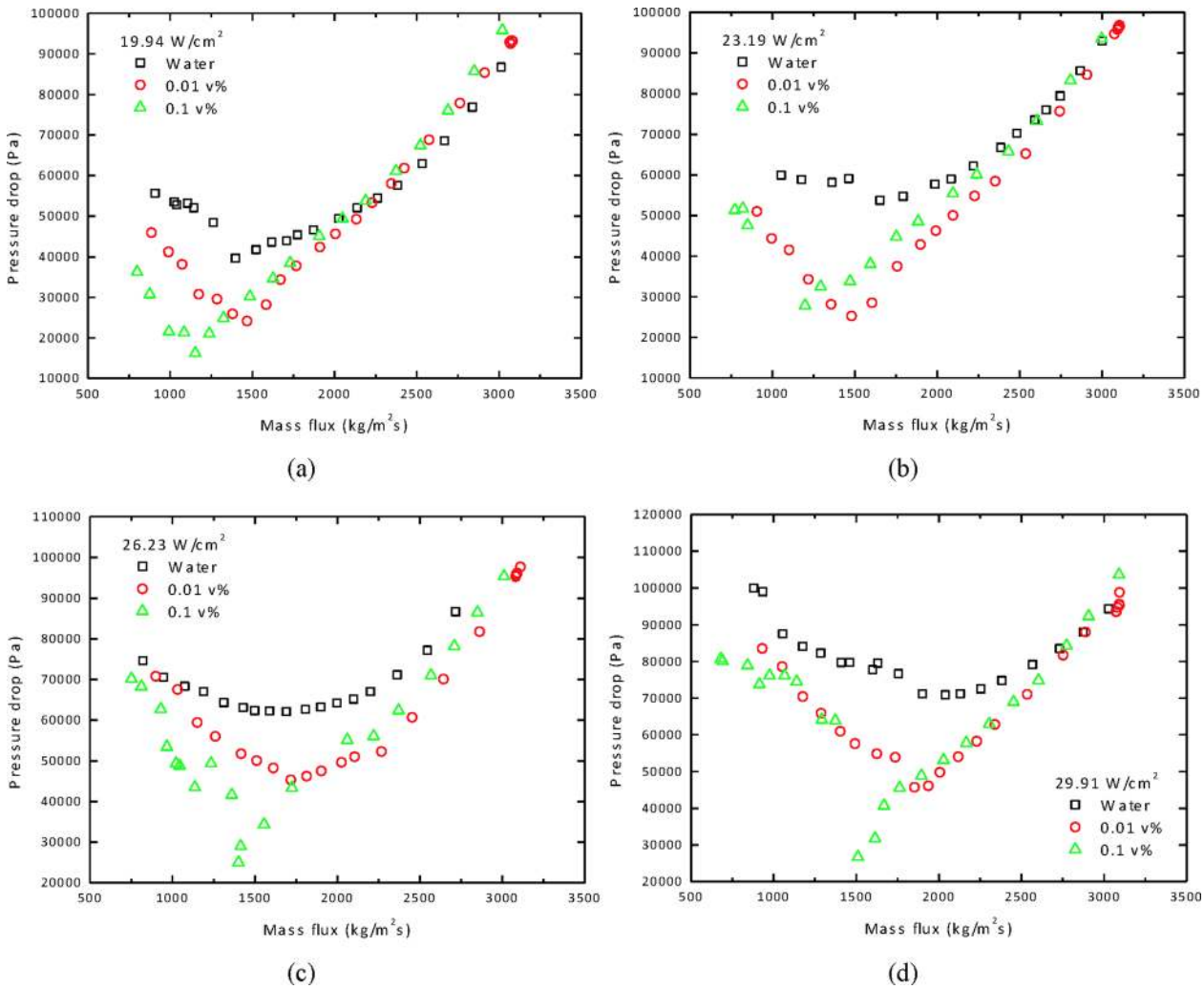

Fig. 11 Comparison of two-phase flow characteristics of water and nanofluids under different heat fluxes. (*a*) $q''_w = 19.9\,W/cm^2$, (*b*) $q''_w = 23.2\,W/cm^2$, (*c*) $q''_w = 26.2\,W/cm^2$, and (*d*) $q''_w = 29.9\,W/cm^2$.

inferred that OFI is delayed in nanofluids; however, once it happens, two-phase flow oscillations will occur abruptly. To better illustrate this, the results in Fig. 10 are recapitulated in Fig. 11, which shows more clearly that at the same heat flux, the OFI shifts toward a lower mass flux and the transition to unstable region becomes more sudden as the nanoparticle concentration increases.

The mechanism responsible for the delayed OFI is probably related to the ONB retardance in nanofluids. As discussed earlier, deposition of nanoparticles on the inner surface of the channel impedes the ONB by reducing the number of available cavities and diminishing the size range of active nucleation sites. Consequently, less amount of vapor is generated during the early stage of flow boiling, and the reduced compressibility in the flow channel suppresses the pressure-drop type oscillations that appear first in two-phase instabilities. However, abrupt nucleation (also generation of large amount of vapor) usually follows the delayed ONB, where the excess thermal energy will be eventually converted to latent heat of the vapor phase as required by energy conservation. This explains the sudden transition of two-phase flow from the stable region to the unstable region in nanofluids.

Conclusions

Forced convective flow boiling and two-phase flow of nanofluids in a minichannel were studied experimentally. It was observed that addition of nanoparticles delays the ONB and suppresses the OFI, and the extent of delay/suppression is proportional to the nanoparticle concentration. These findings were attributed to the changes in available nucleation sites and surface wettability due to nanoparticle deposition on the channel wall as well as the thinning of thermal boundary layer due to the shear-induced nanoparticle redistribution. It was also found that in nanofluids, the pressure-drop type flow instabilities prevail with lesser oscillations in pressure, temperature, and mass flux, and the OFI is impeded by the presence of nanoparticles.

Acknowledgment

The authors acknowledge the financial supports from the Cooling Technologies Research Center (a National Science Foundation Industry/University Cooperative Research Center) at Purdue University and from the National Science Foundation (Grant Nos. 0927340 and 1236606).

Nomenclature

A = inner surface area of channel area, m^2
C = geometric constant
c_p = specific heat, kJ/kg K
D = channel diameter, m
G = mass flux, kg/m^2s
h = heat transfer coefficient, W/m^2 K
h_{fg} = latent heat, kJ/kg

k = thermal conductivity, W/m K
L = length of test tube, m
$\dot{m}$ = mass flow rate, kg/s
p = pressure, kPa
P = pumping power, W
q = heat transfer rate, W
Q = volumetric flow rate, m^3/s
q'' = heat flux, W/m^2
r = cavity radius, μm
T = temperature, °C

Greek Symbols

θ = contact angle
ρ = density, kg/m^3
σ = surface tension, N/m

Subscripts

c = cavity
f = liquid
in = inlet
out = outlet
s = surface
tp = two-phase
v = vapor
w = wall

References

[1] Choi, S. U. S., and Eastman, J. A., 1995, "Enhancing Thermal Conductivity of Fluids With Nanoparticles," 1995 ASME International Mechanical Engineering Congress and Exposition, San Francisco, CA, Nov. 12–17, p. 6.

[2] Choi, S. U. S., Zhang, Z. G., and Keblinski, P., 2004, "Nanofluids," *Encyclopedia of Nanoscience and Nanotechnology*, H. S. Nalwa, ed., American Scientific Pub, Los Angeles, CA.

[3] Yu, W., France, D. M., Routbort, J. L., and Choi, S. U. S., 2008, "Review and Comparison of Nanofluid Thermal Conductivity and Heat Transfer Enhancements," Heat Transfer Eng., **29**(5), pp. 432–460.

[4] Ma, H. B., Wilson, C., Yu, Q., Park, K., Choi, U. S., and Tirumala, M., 2006, "An Experimental Investigation of Heat Transport Capability in a Nanofluid Oscillating Heat Pipe," ASME J. Heat Transfer, **128**(11), pp. 1213–1216.

[5] Ma, H. B., Wilson, C., Borgmeyer, B., Park, K., Yu, Q., Choi, S. U. S., and Tirumala, M., 2006, "Effect of Nanofluid on the Heat Transport Capability in an Oscillating Heat Pipe," Appl. Phys. Lett., **88**(14), p. 143116.

[6] Chen, H., Yang, W., He, Y., Ding, Y., Zhang, L., Tan, C., Lapkin, A. A., and Bavykin, D. V., 2008, "Heat Transfer and Flow Behaviour of Aqueous Suspensions of Titanate Nanotubes (Nanofluids)," Powder Technol., **183**(1), pp. 63–72.

[7] Yang, Y., Zhang, Z. G., Grulke, E. A., Anderson, W. B., and Wu, G., 2005, "Heat Transfer Properties of Nanoparticle-in-Fluid Dispersions (Nanofluids) in Laminar Flow," Int. J. Heat Mass Transfer, **48**(6), pp. 1107–1116.

[8] Wen, D., and Ding, Y., 2004, "Experimental Investigation Into Convective Heat Transfer of Nanofluids at the Entrance Region Under Laminar Flow Conditions," Int. J. Heat Mass Transfer, **47**(24), pp. 5181–5188.

[9] Ding, Y., Alias, H., Wen, D., and Williams, R. A., 2006, "Heat Transfer of Aqueous Suspensions of Carbon Nanotubes (CNT Nanofluids)," Int. J. Heat Mass Transfer, **49**(1–2), pp. 240–250.

[10] He, Y., Jin, Y., Chen, H., Ding, Y., Cang, D., and Lu, H., 2007, "Heat Transfer and Flow Behaviour of Aqueous Suspensions of TiO_2 Nanoparticles (Nanofluids) Flowing Upward Through a Vertical Pipe," Int. J. Heat Mass Transfer, **50**(11–12), pp. 2272–2281.

[11] Zeinali Heris, S., Nasr Esfahany, M., and Etemad, S. G., 2007, "Experimental Investigation of Convective Heat Transfer of Al_2O_3/Water Nanofluid in Circular Tube," Int. J. Heat Fluid Flow, **28**(2), pp. 203–210.

[12] Routbort, J., Singh, D., Timofeeva, E., Yu, W., and France, D., 2011, "Pumping Power of Nanofluids in a Flowing System," J. Nanopart. Res., **13**(3), pp. 931–937.

[13] Corcione, M., Cianfrini, M., and Quintino, A., 2012, "Pumping Energy Saving Using Nanoparticle Suspensions as Heat Transfer Fluids," ASME J. Heat Transfer, **134**(12), p. 121701.

[14] Leyuan, Y., and Dong, L., 2013, "Study of the Thermal Effectiveness of Laminar Forced Convection of Nanofluids for Liquid Cooling Applications," IEEE Compon. Packag. Manuf. Technol., **3**(10), pp. 1693–1704.

[15] Bergman, T. L., 2009, "Effect of Reduced Specific Heats of Nanofluids on Single Phase, Laminar Internal Forced Convection," Int. J. Heat Mass Transfer, **52**(5–6), pp. 1240–1244.

[16] Nguyen, C. T., Desgranges, F., Galanis, N., Roy, G., Maré, T., Boucher, S., and Angue Mintsa, H., 2008, "Viscosity Data for Al_2O_3–Water Nanofluid—Hysteresis: Is Heat Transfer Enhancement Using Nanofluids Reliable?," Int. J. Therm. Sci., **47**(2), pp. 103–111.

[17] Prasher, R., Song, D., Wang, J., and Phelan, P., 2006, "Measurements of Nanofluid Viscosity and Its Implications for Thermal Applications," Appl. Phys. Lett., **89**(13), p. 133108.

[18] Singh, P. K., Anoop, K. B., Sundararajan, T., and Das, S. K., 2010, "Entropy Generation due to Flow and Heat Transfer in Nanofluids," Int. J. Heat Mass Transfer, **53**(21–22), pp. 4757–4767.

[19] Das, S. K., Putra, N., and Roetzel, W., 2003, "Pool Boiling Characteristics of Nano-Fluids," Int. J. Heat Mass Transfer, **46**(5), pp. 851–862.

[20] Das, S. K., Putra, N., and Roetzel, W., 2003, "Pool Boiling of Nano-Fluids on Horizontal Narrow Tubes," Int. J. Multiphase Flow, **29**(8), pp. 1237–1247.

[21] Das, S., Prakash Narayan, G., and Baby, A., 2008, "Survey on Nucleate Pool Boiling of Nanofluids: The Effect of Particle Size Relative to Roughness," J. Nanopart. Res., **10**(7), pp. 1099–1108.

[22] Narayan, G. P., Anoop, K. B., and Das, S. K., 2007, "Mechanism of Enhancement/Deterioration of Boiling Heat Transfer Using Stable Nanoparticle Suspensions Over Vertical Tubes," J. Appl. Phys., **102**(7), p. 074317.

[23] Chopkar, M., Das, A., Manna, I., and Das, P., 2008, "Pool Boiling Heat Transfer Characteristics of ZrO_2–Water Nanofluids From a Flat Surface in a Pool," Heat Mass Transfer, **44**(8), pp. 999–1004.

[24] Vassallo, P., Kumar, R., and D'Amico, S., 2004, "Pool Boiling Heat Transfer Experiments in Silica–Water Nano-Fluids," Int. J. Heat Mass Transfer, **47**(2), pp. 407–411.

[25] Wen, D., and Ding, Y., 2005, "Experimental Investigation Into the Pool Boiling Heat Transfer of Aqueous Based Gamma-Alumina Nanofluids," J. Nanopart. Res., **7**(2–3), pp. 265–274.

[26] Bang, I. C., and Heung Chang, S., 2005, "Boiling Heat Transfer Performance and Phenomena of Al_2O_3–Water Nano-Fluids From a Plain Surface in a Pool," Int. J. Heat Mass Transfer, **48**(12), pp. 2407–2419.

[27] Milanova, D., and Kumar, R., 2005, "Role of Ions in Pool Boiling Heat Transfer of Pure and Silica Nanofluids," Appl. Phys. Lett., **87**(23), p. 233107.

[28] Milanova, D., and Kumar, R., 2008, "Heat Transfer Behavior of Silica Nanoparticles in Pool Boiling Experiment," ASME J. Heat Transfer, **130**(4), p. 042401.

[29] Liu, Z.-h., Xiong, J.-g., and Bao, R., 2007, "Boiling Heat Transfer Characteristics of Nanofluids in a Flat Heat Pipe Evaporator With Micro-Grooved Heating Surface," Int. J. Multiphase Flow, **33**(12), pp. 1284–1295.

[30] Lee, J., and Mudawar, I., 2007, "Assessment of the Effectiveness of Nanofluids for Single-Phase and Two-Phase Heat Transfer in Micro-Channels," Int. J. Heat Mass Transfer, **50**(3–4), pp. 452–463.

[31] Park, K.-J., and Jung, D., 2007, "Enhancement of Nucleate Boiling Heat Transfer Using Carbon Nanotubes," Int. J. Heat Mass Transfer, **50**(21–22), pp. 4499–4502.

[32] Xue, H. S., Fan, J. R., Hu, Y. C., Hong, R. H., and Cen, K. F., 2006, "The Interface Effect of Carbon Nanotube Suspension on the Thermal Performance of a Two-Phase Closed Thermosyphon," J. Appl. Phys., **100**(10), p. 104909.

[33] Kim, H., Kim, J., and Kim, M., 2006, "Experimental Study on CHF Characteristics of Water–TiO_2 Nano-Fluids," Nucl. Eng. Technol., **38**(1), pp. 61–68.

[34] Kim, S. J., Bang, I. C., Buongiorno, J., and Hu, L. W., 2006, "Effects of Nanoparticle Deposition on Surface Wettability Influencing Boiling Heat Transfer in Nanofluids," Appl. Phys. Lett., **89**(15), p. 153107.

[35] Kim, S. J., Bang, I. C., Buongiorno, J., and Hu, L. W., 2007, "Surface Wettability Change During Pool Boiling of Nanofluids and Its Effect on Critical Heat Flux," Int. J. Heat Mass Transfer, **50**(19–20), pp. 4105–4116.

[36] Kim, S. J., McKrell, T., Buongiorno, J., and Hu, L.-W., 2008, "Alumina Nanoparticles Enhance the Flow Boiling Critical Heat Flux of Water at Low Pressure," ASME J. Heat Transfer, **130**(4), p. 044501.

[37] Sefiane, K., 2006, "On the Role of Structural Disjoining Pressure and Contact Line Pinning in Critical Heat Flux Enhancement During Boiling of Nanofluids," Appl. Phys. Lett., **89**(4), p. 044106.

[38] You, S. M., Kim, J. H., and Kim, K. H., 2003, "Effect of Nanoparticles on Critical Heat Flux of Water in Pool Boiling Heat Transfer," Appl. Phys. Lett., **83**(16), pp. 3374–3376.

[39] Xue, H. S., Fan, J. R., Hong, R. H., and Hu, Y. C., 2007, "Characteristic Boiling Curve of Carbon Nanotube Nanofluid as Determined by the Transient Calorimeter Technique," Appl. Phys. Lett., **90**(18), p. 184107.

[40] Liu, D., and Yu, L., 2011, "Single-Phase Thermal Transport of Nanofluids in a Minichannel," ASME J. Heat Transfer, **133**(3), p. 031009.

[41] Steinke, M. E., and Kandlikar, S. G., 2004, "Control and Effect of Dissolved Air in Water During Flow Boiling in Microchannels," Int. J. Heat Mass Transfer, **47**(8–9), pp. 1925–1935.

[42] Yu, L., Liu, D., and Botz, F., 2012, "Laminar Convective Heat Transfer of Alumina-Polyalphaolefin Nanofluids Containing Spherical and Non-Spherical Nanoparticles," Exp. Therm. Fluid Sci., **37**(2), pp. 72–83.

[43] Ramilison, J. M., Sadasivan, P., and Lienhard, J. H., 1992, "Surface Factors Influencing Burnout on Flat Heaters," ASME J. Heat Transfer, **114**(1), pp. 287–290.

[44] Khandekar, S., Joshi, Y. M., and Mehta, B., 2008, "Thermal Performance of Closed Two-Phase Thermosyphon Using Nanofluids," Int. J. Therm. Sci., **47**(6), pp. 659–667.

[45] Coursey, J. S., and Kim, J., 2008, "Nanofluid Boiling: The Effect of Surface Wettability," Int. J. Heat Fluid Flow, **29**(6), pp. 1577–1585.

[46] Ahn, H. S., Kim, H., Jo, H., Kang, S., Chang, W., and Kim, M. H., 2010, "Experimental Study of Critical Heat Flux Enhancement During Forced Convective Flow Boiling of Nanofluid on a Short Heated Surface," Int. J. Multiphase Flow, **36**(5), pp. 375–384.

[47] Kim, S. J., McKrell, T., Buongiorno, J., and Hu, L. W., 2009, "Experimental Study of Flow Critical Heat Flux in Alumina-Water, Zinc-Oxide-Water, and Diamond-Water Nanofluids," ASME J. Heat Transfer, **131**(4), p. 043204.
[48] Taylor, J. R., 1997, *An Introduction to Error Analysis*, University Science Books, New York.
[49] Liu, Z. H., and Qiu, Y. H., 2007, "Boiling Heat Transfer Characteristics of Nanofluids Jet Impingement on a Plate Surface," Heat Mass Transfer, **43**(7), pp. 699–706.
[50] Sheikhbahai, M., Nasr Esfahany, M., and Etesami, N., 2012, "Experimental Investigation of Pool Boiling of Fe_3O_4/Ethylene Glycol–Water Nanofluid in Electric Field," Int. J. Therm. Sci., **62**(12), pp. 149–153.
[51] Nnanna, A. G. A., 2007, "Experimental Model of Temperature-Driven Nanofluid," ASME J. Heat Transfer, **129**(6), pp. 697–704.
[52] Leighton, D., and Acrivos, A., 1987, "The Shear-Induced Migration of Particles in Concentrated Suspensions," J. Fluid Mech., **181**(9), pp. 415–439.
[53] Phillips, R. J., Armstrong, R. C., Brown, R. A., Graham, A. L., and Abbott, J. R., 1992, "A Constitutive Equation for Concentrated Suspensions That Accounts for Shear-Induced Particle Migration," Phys. Fluids A, **4**(1), pp. 30–40.
[54] Hsu, Y. Y., 1962, "On the Size Range of Active Nucleation Cavities on a Heating Surface," ASME J. Heat Transfer, **84**(3), pp. 207–213.
[55] Carey, V. P., 1992, *Liquid-Vapor Phase-Change Phenomena*, Taylor & Francis, New York.
[56] Liu, D., Lee, P.-S., and Garimella, S. V., 2005, "Prediction of the Onset of Nucleate Boiling in Microchannel Flow," Int. J. Heat Mass Transfer, **48**(25–26), pp. 5134–5149.
[57] Bergles, A. E., and Rohsenow, W. M., 1964, "The Determination of Forced-Convection Surface-Boiling Heat Transfer," ASME J. Heat Transfer, **86**(3), pp. 365–372.
[58] Celata, G. P., Cumo, M., and Mariani, A., 1997, "Experimental Evaluation of the Onset of Subcooled Flow Boiling at High Liquid Velocity and Subcooling," Int. J. Heat Mass Transfer, **40**(12), pp. 2879–2885.
[59] Basu, N., Warrier, G. R., and Dhir, V. K., 2002, "Onset of Nucleate Boiling and Active Nucleation Site Density During Subcooled Flow Boiling," ASME J. Heat Transfer, **124**(4), pp. 717–728.
[60] Qu, W., and Mudawar, I., 2002, "Prediction and Measurement of Incipient Boiling Heat Flux in Micro-Channel Heat Sinks," Int. J. Heat Mass Transfer, **45**(19), pp. 3933–3945.
[61] Kakac, S., and Bon, B., 2008, "A Review of Two-Phase Flow Dynamic Instabilities in Tube Boiling Systems," Int. J. Heat Mass Transfer, **51**(3–4), pp. 399–433.
[62] Li, D., Wu, G. S., Wang, W., Wang, Y. D., Liu, D., Zhang, D. C., Chen, Y. F., Peterson, G. P., and Yang, R. G., 2012, "Enhancing Flow Boiling Heat Transfer in Microchannels for Thermal Management With Monolithically-Integrated Silicon Nanowires," Nano Lett., **12**(7), pp. 3385–3390.
[63] Karsli, S., Yilmaz, M., and Comakli, O., 2002, "The Effect of Internal Surface Modification on Flow Instabilities in Forced Convection Boiling in a Horizontal Tube," Int. J. Heat Fluid Flow, **23**(6), pp. 776–791.
[64] Boure, J. A., Bergles, A. E., and Tong, L. S., 1973, "Review of Two-Phase Flow Instability," Nucl. Eng. Des., **25**(2), pp. 165–192.
[65] Kakac, S., 1985, "Two-Phase Flow Instabilities in Boiling Systems: Summary and Review," METU J. Pure Appl. Sci., **18**(2), pp. 171–252.
[66] Neal, L. G., Zivi, S. M., and Wright, R. W., 1967, "The Mechanisms of Hydrodynamic Instabilities in Boiling Channel," Two-Phase Flow Dynamics Symposium: Euratom Report, Eindhoven, The Netherlands, Paper No. 8.1.
[67] Ding, Y., Kakaç, S., and Chen, X. J., 1995, "Dynamic Instabilities of Boiling Two-Phase Flow in a Single Horizontal Channel," Exp. Therm. Fluid Sci., **11**(4), pp. 327–342.
[68] Maulbetsch, J. S., and Griffith, P., 1966, "System Induced Instabilities in Forced Convection Flow With Subcooled Boiling," 3rd International Heat Transfer Conference, Chicago, IL, Aug. 7–12, pp. 247–257.
[69] Stenning, A. H., and Veziroglu, T. N., 1965, "Flow Oscillation Modes in Forced Convection Boiling," Heat Transfer and Fluid Mechanics Institute, Los Angeles, CA, June 21–23, pp. 301–316.
[70] Zhang, T., Wen, J. T., Peles, Y., Catano, J., Zhou, R., and Jensen, M. K., 2011, "Two-Phase Refrigerant Flow Instability Analysis and Active Control in Transient Electronics Cooling Systems," Int. J. Multiphase Flow, **37**(1), pp. 84–97.
[71] Ozawa, M., Nakanishi, S., Ishigai, S., Mizuta, Y., and Tarui, H., 1979, "Flow Instabilities in Boiling Channels: Part I Pressure Drop Oscillation," Bull. JSME, **22**(170), pp. 1113–1118.
[72] Liu, H., 1993, "Pressure-Drop Type and Thermal Oscillations in Convective Boiling Systems," Ph.D. thesis, University of Miami, Miami, FL.